

Perspective

Design of Cu/MoO_x for CO₂ Reduction via Reverse Water Gas Shift Reaction

Yuan Gao^{1,*}, Kun Xiong^{1,*}  and Bingfeng Zhu^{2,*}

¹ Engineering Research Center for Waste Oil Recovery Technology and Equipment, School of Environment and Resources, Ministry of Education, Chongqing Technology and Business University, Chongqing 400067, China

² The First Affiliated Hospital of Chongqing Medical, Pharmaceutical College, Chongqing 400060, China

* Correspondence: kunxiong@ctbu.edu.cn (K.X.); bingfengzhu1978@163.com (B.Z.)

Abstract: CO₂ reduction to CO as raw material for conversion to chemicals and gasoline fuels via the reverse water–gas shift (RWGS) reaction is generally acknowledged to be a promising strategy that makes the CO₂ utilization process more economical and efficient. Cu-based catalysts are low-cost and have high catalytic performance but have insufficient stability due to hardening at high temperatures. In this work, a series of Cu-based catalysts supported by MoO_x were synthesized for noble metal-free RWGS reactions, and the effects of MoO_x support on catalyst performance were investigated. The results show that the introduction of MoO_x can effectively improve the catalytic performance of RWGS reactions. The obtained Cu/MoO_x (1:1) catalyst displays excellent activity with 35.85% CO₂ conversion and 99% selectivity for CO at 400 °C. A combination of XRD, XPS, and HRTEM characterization results demonstrate that MoO_x support enhances the metal-oxide interactions with Cu through electronic modification and geometric coverage, thus obtaining highly dispersed copper and more Cu-MoO_x interfaces as well as more corresponding oxygen vacancies.

Keywords: CO₂ reduction; reverse water–gas shift; Cu-MoO_x; interaction; catalytic performance



Citation: Gao, Y.; Xiong, K.; Zhu, B. Design of Cu/MoO_x for CO₂ Reduction via Reverse Water Gas Shift Reaction. *Catalysts* **2023**, *13*, 684. <https://doi.org/10.3390/catal13040684>

Academic Editor: Concetta Ruocco

Received: 27 February 2023

Revised: 24 March 2023

Accepted: 28 March 2023

Published: 31 March 2023



Copyright: © 2023 by the authors. Licensee MDPI, Basel, Switzerland. This article is an open access article distributed under the terms and conditions of the Creative Commons Attribution (CC BY) license (<https://creativecommons.org/licenses/by/4.0/>).

1. Introduction

In recent years, with the increase in CO₂ emissions, the greenhouse effect has become increasingly serious, which has led to a series of natural disasters, causing widespread global attention to the field of CO₂ capture, conversion, and utilization [1–3]. At present, carbon capture and storage (CCS) have been successfully used to reduce greenhouse gas emissions directly into the atmosphere by geological, mineralization, or oceanic means, but CO₂, as a rich and cheap carbon source, has not been effectively utilized [4,5]. CO₂ reduction to CO as raw material for conversion to chemicals and gasoline fuels via the reverse water–gas shift (RWGS) reaction is generally acknowledged to be a promising strategy that makes the CO₂ utilization process more economical and efficient on a large industrial scale and realizes a good carbon cycle [6].

However, the high stability of CO₂, the endothermic characteristics, thermodynamically favorable at high reaction temperatures, and the additional side reactions inhibit the industrialization of the RWGS reaction. Therefore, it is a great challenge to design high-activity and selectivity catalysts at a mild temperature range. At present, researchers and institutions mainly focus on the catalytic performance of metal catalysts [7,8], metal oxide catalysts [9–11], and transition metal carbides [12–14] for RWGS reactions. Su et al. systematically studied the CO₂ hydrogenation on a Pt (111) surface and revealed that CO₂ can be activated on a clean Pt (111) surface through the dissociation mechanism to form adsorbed CO and O at room temperature and at high temperatures [15]. Xu et al. reported that K doping changed the chemical states of Mo and Cu through interface interaction and electron transfer, resulting in improved adsorption and activation performances of CO₂ on the K-promoted Cu/β-Mo₂C catalysts [16]. Nickel-based catalysts can effectively catalyze the RWGS reaction, but their selectivity toward CO at low temperatures is poor.

Researchers found that RWGS reactions and product selectivity can be adjusted by surface modification of Ni. The added MoO_x and Ni have an interface effect, which improves the selectivity of CO through both geometric coverage and electronic modification [17].

Copper-based catalysts are very well-known for their high catalytic activity and low price, but the high temperature hardening and instability hinder their usefulness [18]. Cu catalysts often improve catalytic performance by combining with oxide materials, which will modify the surface of copper and promote the dispersion of copper particles, form strong interface interactions between Cu and oxides, and affect the chemical state of Cu through electronic transfer. The copper was deposited on silica to obtain highly dispersed nano-Cu/SiO₂ catalysts. The catalyst has abundant acid sites and a specific surface area, which is beneficial for improved MTHF selectivity [19]. CeO₂ and Fe₂O₃ are usually used as effective redox and textural promoters to form metal–metal oxide interfaces with Cu, which can boost oxygen vacancies and dispersion of the metal to facilitate the RWGS reaction [20–22]. Molybdenum oxide can be pre-reduced to obtain MoO_x with oxygen defects on the surface and adjust its surface electronic structure. Using MoO_x as the support for Cu catalysis, driven by the control of defect engineering, the Cu/MoO_x catalyst surface will produce more surface metal atoms with low coordination, which will improve the binding ability of the material surface with other atoms, ions, or small molecules. Moreover, the introduction of MoO_x will form new oxygen vacancies in Cu/MoO_x materials through electronic modification, and oxygen vacancies are often related to greater RWGS reaction activity [23]. Therefore, understanding how the structure and properties of the Cu/MoO_x catalysts affect the activity and selectivity of CO₂ reduction helps to design more efficient catalysts for the RWGS reaction.

In this study, a series of Cu-based catalysts supported by MoO_x were synthesized by the hydrothermal method for noble metal-free RWGS reactions. A combination of XRD, XPS, and HRTEM characterization results demonstrate that MoO_x support enhances the metal-oxide interactions with Cu through electronic modification and geometric coverage, thus obtaining highly dispersed copper and more Cu-MoO_x interfaces as well as more corresponding oxygen vacancies. The introduction of MoO_x can effectively improve the catalytic performance of Cu/MoO_x in the RWGS reaction.

2. Results and Discussion

2.1. Catalyst Characterization

XRD patterns of Cu/MoO_x catalysts pre-reduced at 450 °C for 2 h with different atomic ratios of Cu/Mo (1:2, 1:1, and 2:1) are displayed in Figure 1. Two diffraction peaks at approximately 43.3° and 50.5° are observed for all samples, which are attributed to the (111) and (200) planes of the cubic Cu phase (JCPDS No. 04-0836). At the same time, mixed phases of monoclinic MoO₂ (JCPDS No. 32-0671) and hexagonal MoO₃ (JCPDS No. 21-0569) can also be obtained in Cu/MoO_x with different atomic ratios of Cu/Mo. When Cu/Mo is 2:1, there is (NH₄)₂Mo₄O₃ (2θ = 15.1°, 30.2°) as an impurity phase. Due to the high concentration of Cu²⁺ in the system consumed H⁺, the reaction between H⁺ and (Mo₇O₂₄)⁶⁻ is incomplete, and the intermediate state (NH₄)₂Mo₄O₃ appears [24].

Typical SEM micrographs of Cu/MoO_x samples with different atomic ratios of Cu/Mo are shown in Figure 2. The SEM images clearly show the difference in the microstructure of the Cu/MoO_x powder with different atomic ratios. The Cu/MoO_x powders with a Cu/Mo ratio of 1:1 (Figure 2b,e) show micro/nano structures formed by loose sheets and particles. The particle size distribution is from 0.2 μm to 2.5 μm with many holes and caves. This micro/nano porous structure provides a larger specific surface area and more active sites, which is beneficial for the transportation of reactants and products in the reaction process. When Cu/Mo ratios are 1:2 and 2:1, the two samples appear to be composed of more widely distributed and irregular particles with smooth surfaces, as shown in Figure 2a,d,c,f.

Figure 3a is the TEM image of Cu/MoO_x (1:1). Several sheet-like morphologies in Cu/MoO_x ranging from several tens to hundreds of nanometers of particulates exhibit close contact, which enhances the interaction between Cu and MoO_x. To analyze the

crystalline structural details of the nanoparticles, HRTEM is measured and shown in Figure 3b. Cu/MoO_x catalyst shows three distinct lattice fringes of 0.210 nm, 0.343 nm, and 0.347 nm, which correspond to characteristic Cu (111), MoO₂ (−111), and MoO₃ (210) planes, respectively. Moreover, it can be seen that the Cu/MoO_x catalyst contains abundant Cu-MoO_x interfaces, which is attributed to the close contact between the small size of metallic Cu and MoO_x nanoparticles.

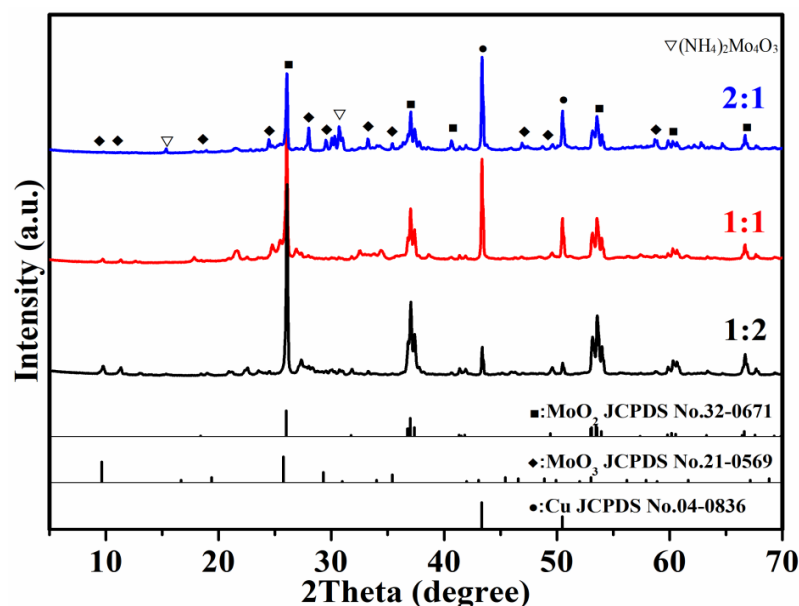


Figure 1. XRD patterns of Cu/MoO_x samples pre-reduced at 450 °C for 2 h.

The interaction between Cu and MoO_x was investigated by using H₂–TPR. As shown in Figure 4, a reduction peak for MoO_x is observed at 620 °C, which is related to the reduction of MoO₃ to MoO₂. The effect of copper addition to MoO_x is largely beneficial for overall reducibility. Cu/MoO_x exhibits significantly larger peaks and is shifted to lower temperatures compared to the MoO_x. It can be attributed to the copper-support interaction at the interface of copper and MoO_x, which has a beneficial effect on the redox property of Cu/MoO_x precursors [25]. For Cu/MoO_x precursors with different atomic ratios of Cu/Mo, the first reduction peak shifts to a higher temperature compared with pure Cu. This trend indicates that the MoO_x stabilizes the Cu species [17]. As can be seen in Figure 4, the Cu/MoO_x (1:1) shows the lowest reduction temperatures. The two main reduction peaks are located at 330 °C and 380 °C, indicating that it is more easily reduced. However, with increasing Cu proportion (Cu/Mo ratio of 2:1), the reduction peak gradually moves towards higher temperatures. The excessive CuO can induce aggregation and overlap of Cu species on the surface of the precursor in the process of calcination and obstruct the pores of MoO_x, which blocks the entry of H₂ [26]. This is consistent with the results of SEM. As a result, the reducibility of the corresponding precursor is gradually weakened. It is worth noting that the reduction peak temperature of the catalyst (Cu:Mo = 1:2) moves higher and the peak area is relatively smaller, indicating that Mo species cannot be reduced completely to the metallic state and a lower Mo/Cu ratio corresponds to a higher reduction degree of the Mo species [27].

X-ray photoelectron spectroscopy (XPS) was utilized to study the surface element composition and the existing state of surface elements. The XPS spectrum of Cu/MoO_x is shown in Figure 5 and Table 1. The metal content is close to the theoretical ratios. It is feasible to synthesize Cu-based catalysts supported on MoO_x in different proportions by the hydrothermal method. Further, the N₂ adsorption-desorption isotherms analysis shows that the specific surface area is 146.0, 156.7, and 117.5 m² g^{−1} for Cu/MoO_x catalysts with Cu/Mo ratios of 1:2, 1:1, and 2:1, respectively. The materials are mesoporous, with a variation in BJH pore diameter of 9–17 nm.

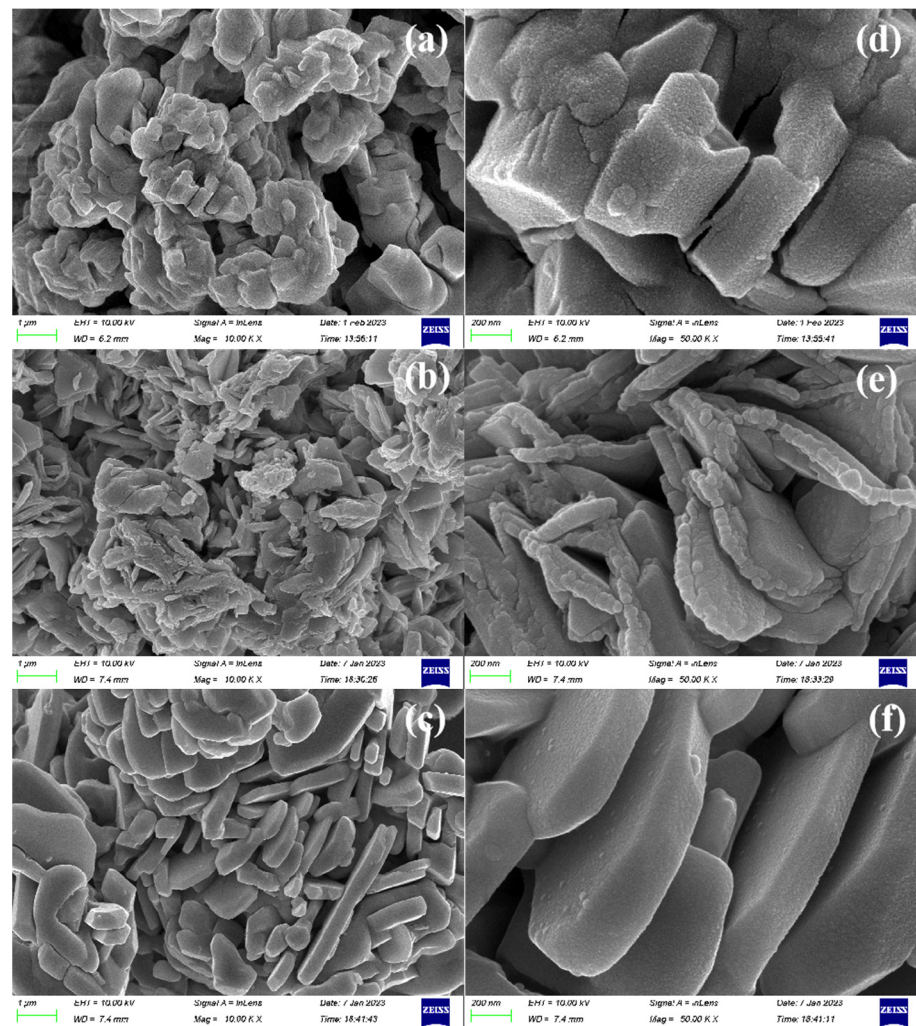


Figure 2. SEM images of Cu/MoO_x samples with different atomic ratios of Cu/Mo (a,d) 1:2, (b,e) 1:1, and (c,f) 2:1.

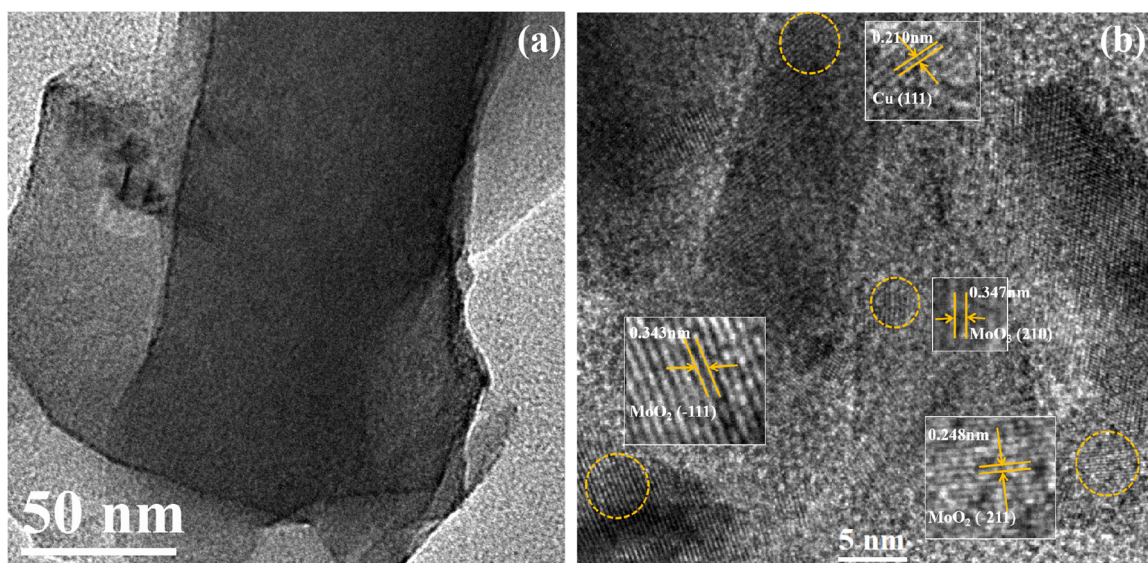


Figure 3. The TEM (a) and HRTEM (b) images of Cu/MoO_x (1:1) catalyst.

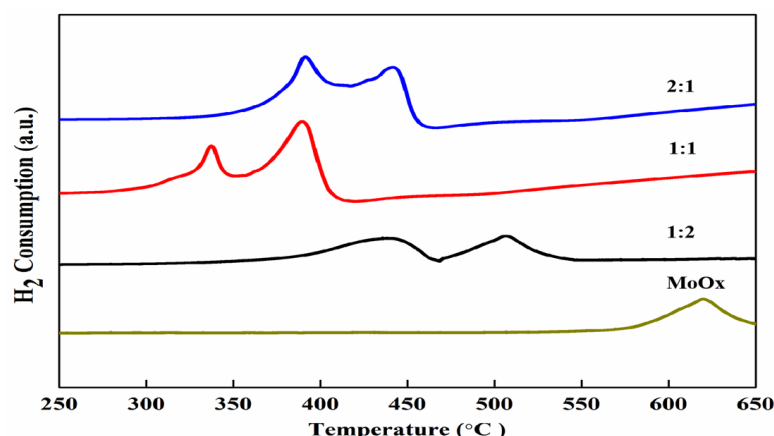


Figure 4. H₂–TPR profiles of pre-reduced Cu/MoO_x and MoO_x at 450 °C under the flow of 4% H₂/Ar mixture gas for 2 h.

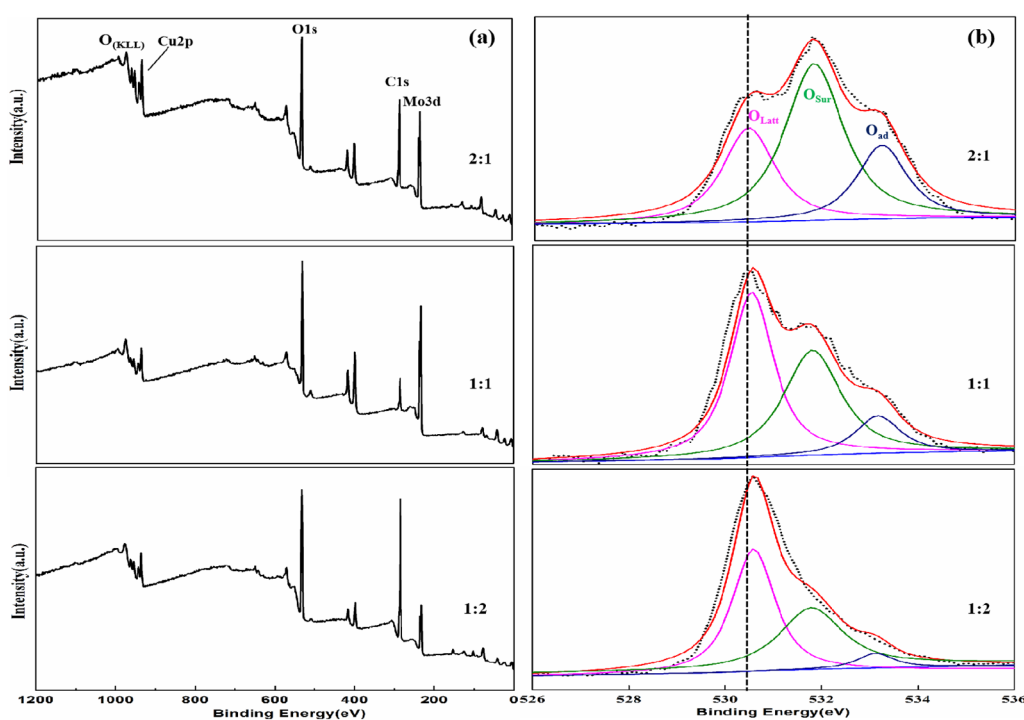


Figure 5. (a) Survey X-ray photoelectron spectra for Cu/MoO_x as well as the core level of (b) O1s spectra.

Table 1. Atomic composition by XPS, surface area, and pore size distribution.

Catalysts	Surface Composition by XPS (at%)				Physicochemical Properties	
	Cu	Mo	O	C	S _{BET} (m ² g ^{−1})	X _{Pd} (nm)
Cu/MoO _x (1:2)	7.17	12.06	48.99	31.77	146.0	11.30
Cu/MoO _x (1:1)	6.28	5.83	36.4	51.48	156.7	9.32
Cu/MoO _x (2:1)	4.28	2.99	31.91	60.81	117.5	17.02

As can be seen in Figure 5a, the Cu, Mo, and O are identified for all the Cu/MoO_x catalysts without impurities on the surface of the compositions. The standard peak of C 1s is at 284.78 eV as the reference. Figure 5b is the O1s XPS spectra of the studied Cu/MoO_x catalysts. The XPS of O1s can be deconvoluted into three major peaks. The peak at 529.5–530.5 eV corresponds to lattice oxygen (O_{Latt}) enclosed by either copper or molybdenum; a higher binding energy peak at 531.0–532.0 eV is related to the surface oxygen (O_{Sur}) atom or

OH, COOH group attached, whereas the peak at 533.5 eV may be due to the presence of adsorbed H₂O in the Cu/MoO_x nanocomposite [28,29]. Compared with the Cu/MoO_x sample with a Cu/Mo ratio of 2:1, the O_{Latt} XPS peaks of two other catalysts with a Cu/Mo ratio of 1:1 and 1:2 obviously shift to the high binding energy direction. This may be due to the increased molybdenum content significantly increasing the content of Mo⁴⁺ and Mo⁶⁺ species in Cu/MoO_x catalysts, and the Mo⁴⁺ species changing the chemical environment of O_{Latt} species [30]. The transfer of electrons from the relatively electron-rich d band of Cu to MoO_x species is realized through the strong electronic interaction between Cu and MoO_x. Compared with the catalysts with a Cu/Mo ratio of 2:1 and 1:2, the catalyst with a Cu/Mo ratio of 1:1 has a larger O_{Latt} XPS peak area and a smaller O_{Sur} XPS peak area. The catalyst with a Cu/Mo ratio of 1:1 has a lower O_{Sur}/O_{Latt} value, indicating that there are more oxygen vacancies in the sample. The oxygen vacancies are considered to be the main active sites for CO₂ catalytic hydrogenation, which may lead to superior catalytic performances of Cu/MoO_x (1:1) catalysts in CO₂ hydrogenation reduction reactions [31].

The XPS spectra of Mo in Cu/MoO_x are shown in Figure 6. Two distinct peaks centered at 232.00 eV and 235.60 eV are consistent with Mo⁴⁺ 3d_{5/2} and Mo⁶⁺ 3d_{5/2}, and according to the previous references and the standard XPS spectrum for MoO_x (x = 2~3) (Mo⁴⁺ 3d_{5/2} at 232.4 eV, Mo⁶⁺ 3d_{5/2} at 236.0 eV), the oxidation state of Mo is Mo (IV) and (VI) [32–34]. The results are consistent with the XRD measurement: Cu/MoO_x (x = 2~3) is a functional heterostructure material. Increasing the Mo/Cu ratio results in a shift of peaks to a higher value, and we speculate that the electron transfer from Cu to MoO_x species occurred due to strong electronic interactions between Cu and MoO_x species.

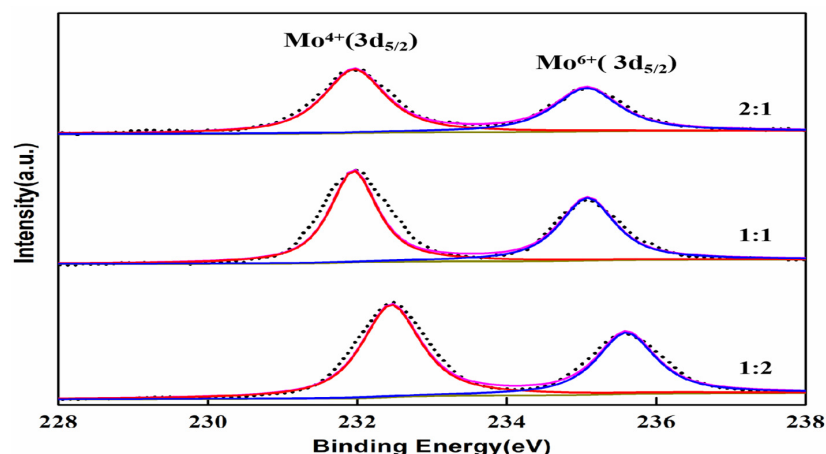


Figure 6. The deconvoluted peaks of Mo3d in Cu/MoO_x samples.

2.2. Catalytic Performance

The performance of the Cu/MoO_x catalyst was investigated by the RWGS reaction with an H₂/CO₂ ratio of 4:1 from 200 °C to 400 °C at 1 bar. As depicted in Figure 7, the CO₂ conversion of three samples increases with the reaction temperature rising, evidencing an endothermic process of the RWGS reaction. Below 280 °C, the catalysts (Cu:Mo = 2:1) have a higher CO₂ conversion because Cu⁰ is the main active site for RWGS. The catalyst with a Cu/Mo ratio of 1:1 displays the best catalytic activity, showing 35.85% CO₂ conversion at 400 °C. Obviously, the support from MoO_x can affect the catalytic activity. Metal-oxide interactions have been considered to play a crucial role in the reactivity of supported catalysts [35,36].

In this study, the interaction between Cu and MoO_x should also be responsible for the improved activity because it will promote the high dispersion of Cu and produce more Cu-MoO_x interfaces as well as more corresponding oxygen vacancies [37]. As stated above, TEM images of Cu/MoO_x (1:1) show affluent Cu-MoO_x interfaces. Because MoO_x modifies the surface of Cu particles through both geometric coverage and electronic modification, XPS results also show that the Cu/MoO_x (1:1) catalyst has more oxygen vacancies. Highly

dispersed Cu and more oxygen vacancies lead to large active surfaces and more active points for CO₂ catalytic hydrogenation. In terms of CO selectivity, the Cu/MoO_x (1:2) catalyst shows high selectivity for CO at low temperatures. No impurity products are found in the system, and CO selectivity is up to 100%. In contrast, Cu/MoO_x (2:1) shows poor CO selectivity of 97.4%. These results suggest that the reduced MoO_x is capable of dissociating CO₂, and the low activity is possibly related to the low ability of MoO_x for H₂ activation and hydrogenation, resulting in a change in the selectivity of the RWGS [17].

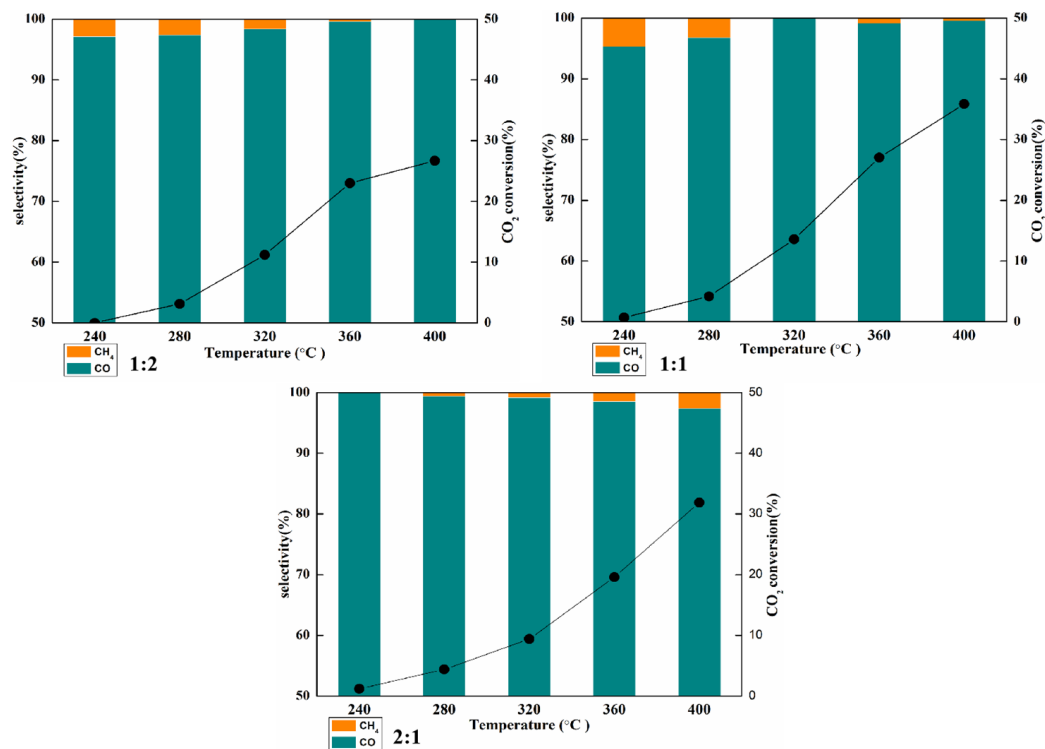


Figure 7. CO₂ conversion, CO selectivity, and CH₄ selectivity for Cu/MoO_x catalysts in the RWGS process as a function of temperature.

According to the literature, there are two reaction mechanisms for the RWGS reaction that have been widely accepted, namely, the redox mechanism and the decomposition intermediate species (carbonate, formate, carbonyl, etc.) mechanism. Based on the previous research, we speculate that the reverse water gas reaction may experience an associative mechanism. The reaction process is as follows: (I) H₂ is activated and adsorbed on the surface of Cu (111). (II) CO₂ reacts with the oxygen vacancies on Cu/MoO_x. (III) H₂ dissociates and spills over the H atoms to the intermediate, leading to the formed formates (HCOO*) of intermediate species. (IV) The formates (HCOO*) dissociate to CO, adsorbed OH, and linear CO (L-CO), which adsorb on Cu. (V) The linear CO (L-CO) desorbs to CO, and the formed OH reacts with the H atom to form H₂O.





A comparison of Cu/MoO_x (1:1) with the recently reported catalysts for RGWS is displayed in Table 2. In terms of CO₂ conversion, our catalyst shows comparatively better activity than the recently reported catalyst under the same reduction reaction conditions. Although CO selectivity is not the highest, Cu/MoO_x (1:1) delivers a competitive selectivity of 99%.

Table 2. Cu/MoO_x (1:2) catalyst performance comparison with the recent reports in the literature.

Catalysts	H ₂ :CO ₂	Temperature (°C)	CO ₂ Conversion	CO Selectivity	Ref.
Cu/MoO _x (1:2)	4	400	35.9%	99.0%	This work
1K-Cu/β-Mo ₂ C	4	400	24.8%	99.5%	[16]
Mo/β-Mo ₂ C	4	400	3.8%	96.5%	[16]
Au/Al ₂ O ₃	4	400	11.0%	100%	[38]
Pt/SiO ₂	4	400	12.1%	100%	[39]
Pt-O.5Re/SiO ₂	4	400	24.3 %	97.3%	[39]
Cu/CeO ₂	4	400	31%	100%	[40]
Cu-Ce/CDC	4	400	24.2%	98.4%	[3]
Ni-1Mo	4	400	23.6%	93.8%	[41]
FeCu/CeAl	4	400	23.6%	96.7%	[42]

3. Experimental Section

3.1. Catalyst Preparation

The Cu/MoO_x catalysts were synthesized by a hydrothermal method, followed by solid-phase sintering. Cu/MoO_x precursors were prepared by dissolving stoichiometric amounts of Cu(NO₃)₂·3H₂O and (NH₄)₆Mo₇O₂₄·4H₂O in deionized water to form a solution. To assess the influences of catalyst components on the morphology, size, and catalytic performance, the molar ratios of Cu:Mo are 1:1, 1:2, and 2:1, respectively. The resulting solution was transferred into a 100 mL Teflon-lined stainless steel autoclave and sealed and heated at 180 °C for 6 h. The precursors were collected by filtration and dried at 80 °C in a vacuum oven. The obtained precursor was calcined at 450 °C for 2 h under flowing 4% H₂/Ar mixture gas to make it pre-reduced and obtain a stable morphology. The preparation process of Cu/MoO_x catalyst is shown in Figure 8.

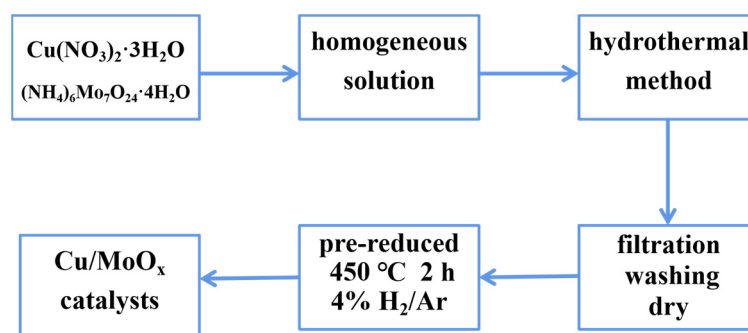


Figure 8. The pattern of Cu/MoO_x catalyst preparation process.

3.2. Product Characterization

The X-ray diffraction (XRD, MO3xHF22, MacScience, Tokyo, Japan) data were obtained to determine material structural properties under the conditions of Cu K radiation with a speed of 1 °C min⁻¹ and the scanning range (2θ) from 10.0° to 80.0°. Nitrogen adsorption was measured in a Tristar 3000 analyzer (Micrometrics, Ottawa, ON, Canada) at liquid nitrogen temperature. The samples were pretreated at 300 °C under a vacuum prior to measurements. The specific surface area of the catalysts was calculated using the

Brunauer–Emmett–Teller (BET) method. X-ray photoelectron spectroscopy (XPS, Thermo VG Scientific Co., Ltd., Waltham, MA, USA) was conducted to analyze the valence states of elements in Cu/MoO_x. The basic characteristics of the catalysts were studied with hydrogen temperature-programmed reduction (H₂-TPR). In a typical experiment, 50 mg of samples was loaded in a fixed-bed quartz reactor, then heated to 300 °C at a rate of 10 °C min⁻¹ in an Ar flow (25 mL min⁻¹) for 1 h to clean the sample. The experiment was carried out in a 5% H₂/Ar flow of 25.0 mL·min⁻¹, with heating to 700 °C at a heating rate of 10 °C min⁻¹. The hydrogen consumption of samples during the heating process was recorded by gas chromatography equipped with a TCD detector. Scanning electron microscopy (SEM, SIGMA 500, Zeiss, Oberkochen, Germany) and transmission electron microscopy (TEM, JEM 2100F, JEOL, Tokyo, Japan) were utilized to observe the morphology of catalysts.

3.3. Catalytic Evaluation

The catalytic performance of the Cu/MoO_x catalyst was evaluated by the CO₂ reverse water-gas shift (RWGS) reaction. The RWGS reaction was carried out in a quartz fixed-bed microreactor with an internal diameter of 6 mm under atmospheric pressure. Before the reaction, the catalysts were initially reduced by H₂ 50 mg as prepared samples were put into the quartz tube, which is placed in the tubular furnace, and then reduced at 400 °C for 2 h using pure H₂ (15 mL min⁻¹, atmospheric pressure). Next, the inlet flow was changed to 20 mL min⁻¹ Ar for cooling down to 200 °C, and then the inlet flow was switched to a 50.0 mL min⁻¹ CO₂/H₂/Ar mixture gas (10/40/50) for CO₂ hydrogenation. The temperature range of the catalyst's activity test is from 200 °C to 400 °C. The concentration of gas products was analyzed online by gas chromatography equipped with a thermal conductivity detector (TCD) and a flammable ionization detector (FID), and the chromatographic column model is TDX-01. The CO₂ conversion (X_{CO_2} , %), selectivity to CO (S_{CO} , %), and selectivity to CH₄ (S_{CH_4} , %) were defined following Formulas (1)–(3):

$$\text{CO}_2 \text{ Conversion} = \frac{[\text{CO}_2]_{\text{inlet}} - [\text{CO}_2]_{\text{outlet}}}{[\text{CO}_2]_{\text{inlet}}} \times 100\% \quad (1)$$

$$\text{CO Selectivity} = \frac{[\text{CO}]_{\text{outlet}}}{[\text{CO}]_{\text{outlet}} + [\text{CH}_4]_{\text{outlet}}} \times 100\% \quad (2)$$

$$\text{CH}_4 \text{ Selectivity} = \frac{[\text{CH}_4]_{\text{outlet}}}{[\text{CO}]_{\text{outlet}} + [\text{CH}_4]_{\text{outlet}}} \times 100\% \quad (3)$$

4. Conclusions

A series of Cu-based catalysts supported on MoO_x were synthesized by the hydrothermal method for noble metal-free RWGS reactions. MoO_x support enhances the metal-oxide interactions with Cu through electronic modification and geometric coverage. As a result, MoO_x support improves the high dispersion of Cu and produces more Cu-MoO_x interfaces as well as more corresponding oxygen vacancies. The Cu/MoO_x (1:1) displays excellent catalytic performance with 35.85% CO₂ conversion and 99% selectivity for CO at 400 °C. The Cu/MoO_x as a non-noble metal catalyst shows great potential in the RWGS reaction used as an industrially developed process at a medium-low temperature.

Author Contributions: Data curation, Y.G.; formal analysis, Y.G. and B.Z.; investigation, Y.G. and K.X.; resources, Y.G. and B.Z.; supervision, B.Z.; writing—original draft, Y.G.; writing—review and editing, Y.G. All authors have read and agreed to the published version of the manuscript.

Funding: This research was funded by the Science and Technology Project from the Chongqing Education Commission (Grant No. KJQN2019008832), the Natural Science Foundation Project of Chongqing (Grant No. cstc2020jcyj-msxmX0345 and CSTB2022NSCQ-MSX1230), and the Research Platform Open Project of the Chongqing Technology and Business University (No. KFJJ2019086).

Data Availability Statement: Not applicable.

Conflicts of Interest: The authors declare no conflict of interest.

References

1. Wang, W.H.; Himeda, Y.; Muckerman, J.T.; Manbeck, G.F.; Fujita, E. CO₂ Hydrogenation to Formate and Methanol as an Alternative to Photo- and Electrochemical CO₂ Reduction. *Chem. Rev.* **2015**, *115*, 12936–12973. [[CrossRef](#)] [[PubMed](#)]
2. Fu, J.; Jiang, K.; Qiu, X.; Yu, J.; Liu, M. Product selectivity of photocatalytic CO₂ reduction reactions. *Mater. Today* **2020**, *32*, 222–243. [[CrossRef](#)]
3. Wang, X.X.; Duan, Y.H.; Zhang, J.F.; Tan, Y.S. Catalytic Conversion of CO₂ into High Value-Added Hydrocarbons over Tandem Catalyst. *J. Fuel Chem. Technol.* **2022**, *50*, 538–563. [[CrossRef](#)]
4. Chen, J.; Duan, L.; Sun, Z. Review on the development of sorbents for calcium looping. *Energy Fuels* **2020**, *34*, 7806–7836. [[CrossRef](#)]
5. Leeson, D.; Mac Dowell, N.; Shah, N.; Petit, C.; Fennell, P. A Techno-economic analysis and systematic review of carbon capture and storage (CCS) applied to the iron and steel, cement, oil refining and pulp and paper industries, as well as other high purity sources. *Int. J. Greenh. Gas Control* **2017**, *61*, 71–84. [[CrossRef](#)]
6. Oshima, K.; Shinagawa, T.; Nogami, Y. Low temperature catalytic reverse water gas shift reaction assisted by an electric field. *Catal. Today* **2014**, *232*, 27–32. [[CrossRef](#)]
7. Rodriguez, J.A.; Ma, S.; Liu, P.; Hrbek, J.; Evans, J.; Perez, M. Activity of CeO_x and TiO_x Nanoparticles Grown on Au(111) in the Water-Gas Shift Reaction. *Science* **2007**, *318*, 1757–1760. [[CrossRef](#)] [[PubMed](#)]
8. Chen, X.; Su, X.; Su, H.; Liu, X.; Miao, S.; Zhao, Y.; Sun, K.; Huang, Y.; Zhang, T. Theoretical insights and the corresponding construction of supported metal catalysts for highly selective CO₂-to-CO conversion. *ACS Catal.* **2017**, *7*, 4613–4620. [[CrossRef](#)]
9. Park, S.W.; Joo, O.S.; Jung, K.D.; Kim, H.; Han, S.H. Development of ZnO/Al₂O₃ catalyst for reverse-water-gas-shift reaction of CAMERE (carbon dioxide hydrogenation to form methanol via a reverse-water-gas-shift reaction) process. *Appl. Catal. A* **2001**, *211*, 81–90. [[CrossRef](#)]
10. Zonetti, P.C.; Letichevsky, S.; Gaspar, A.B.; Sousa-Aguiar, E.F.; Appel, L.G. The Ni_xCe_{0.75}Zr_{0.25-x}O₂ solid solution and the RWGS. *Appl. Catal. A* **2014**, *475*, 48–54. [[CrossRef](#)]
11. Silva-Calpa, L.D.R.; Zonetti, P.C.; Rodrigues, C.P.; Alves, O.C.; Appel, L.G.; Avillez, R.R.de. The Zn_xZr_{1-x}O_{2-y} solid solution on m-ZrO₂: Creating O vacancies and improving the m-ZrO₂ redox properties. *J. Mol. Catal. A Chem.* **2016**, *425*, 166–173. [[CrossRef](#)]
12. Rodriguez, J.A.; Liu, P.; Stacchiola, D.J.; Senanayake, S.D.; White, M.G.; Chen, J.G. Hydrogenation of CO₂ to Methanol: Importance of Metal-Oxide and Metal-Carbide Interfaces in the Activation of CO₂. *ACS Catal.* **2015**, *5*, 6696–6706. [[CrossRef](#)]
13. Andrés, A.G.B.; Octavio, J.F.; Dario, J.S.; Karim, S.; Marcelo, S.N. Porous Mo_xC_y/SiO₂ Material for CO₂ Hydrogenation. *Top. Catal.* **2019**, *62*, 1026–1034.
14. Zhang, X.; Zhu, X.; Lin, L.; Yao, S.; Zhang, M.; Liu, X.; Wang, X.; Li, Y.; Shi, C.; Ma, D. Highly Dispersed Copper over β-Mo₂C as an Efficient and Stable Catalyst for the Reverse Water Gas Shift (RWGS) Reaction. *ACS Catal.* **2017**, *7*, 912–918. [[CrossRef](#)]
15. Su, H.; Ye, Y.; Lee, K.J.; Zeng, J.; Mun, B.S.; Crumlin, E.J. Probing the surface chemistry for reverse water gas shift reaction on Pt (1 1 1) using ambient pressure X-ray photoelectron spectroscopy. *J. Catal.* **2020**, *391*, 123–131. [[CrossRef](#)]
16. Xu, J.J.; Gong, X.X.; Hu, R.R.; Liu, Z.W.; Liu, Z.T. Highly active K-promoted Cu/β-Mo₂C catalysts for reverse water gas shift reaction: Effect of potassium. *Mol. Catal.* **2021**, *516*, 111954. [[CrossRef](#)]
17. Zhang, R.Y.; Wei, A.L.; Zhu, M.; Wu, X.X.; Wang, H.; Zhu, X.L.; Ge, Q.F. Tuning reverse water gas shift and methanation reactions during CO₂ reduction on Ni catalysts via surface modification by MoO_x. *J. CO₂ Util.* **2021**, *52*, 101678. [[CrossRef](#)]
18. Noelia, L.G.; Jannier, C.; Jose, M.P. Graphene-TLL-Cu₂ONPs Hybrid as Highly Efficient Catalyst for Degradation of Organic Compounds. *Nanomaterials* **2023**, *13*, 449.
19. Ramyakrishna, P.; Prathap, C.; Rajendiran, R.; Rajender, B.; Ravi, B.; Putrakumar, B.; Vijayanand, P.; Ahmed, B.R.; Aboubakr, M.A.; Noora, A.Q. Vapour-Phase Selective Hydrogenation of γ-Valerolactone to 2-Methyltetrahydrofuran Biofuel over Silica-Supported Copper Catalysts. *Nanomaterials* **2022**, *12*, 3414.
20. Gonzalez-Castano, M.; Navarro de Miguel, J.C.; Sinha, F.; Ghomsi, W.S.; Klepel, H. Cu supported Fe-SiO₂ nanocomposites for reverse water gas shift reaction. *J. CO₂ Util.* **2021**, *46*, 101493. [[CrossRef](#)]
21. Chen, L.; Wu, D.; Wang, C.; Ji, M.; Wu, Z. Study on Cu-Fe/CeO₂ bimetallic catalyst for reverse water gas shift reaction. *J. Environ. Chem. Eng.* **2021**, *9*, 105183. [[CrossRef](#)]
22. Yang, L.; Pastor-Perez, L.; Villora-Pico, J.J.; Sepúlveda-Escribano, A.; Tian, F.; Zhu, M. Highly Active and Selective Multicomponent Fe-Cu/CeO₂-Al₂O₃ Catalysts for CO₂ Upgrading via RWGS: Impact of Fe/Cu Ratio. *ACS Sustain. Chem. Eng.* **2021**, *9*, 101493. [[CrossRef](#)]
23. Zhang, B.W.; Cao, L.C.; Tang, C.; Tan, C.H.; Cheng, N.Y.; Lai, W.H.; Wang, Y.X.; Cheng, Z.X.; Dong, J.C.; Kong, Y.; et al. Atomically Dispersed Dual-Site Cathode with a Record High Sulfur Mass Loading for High-Performance Room-Temperature Sodium–Sulfur Batteries. *Adv. Mater.* **2023**, *35*, 2206828. [[CrossRef](#)] [[PubMed](#)]
24. Song, J.M.; Ni, X.M.; Zhang, D.E. Fabrication and photoluminescence properties of hexagonal MoO₃ rods. *Solid State Sci.* **2006**, *8*, 1164–1167. [[CrossRef](#)]

25. Qi, T.Q.J.; Li, W.Z.; Li, H.; Jia, K.; Chen, S.Y.; Zhang, Y.C. Yttria-doped Cu/ZnO catalyst with excellent performance for CO₂ hydrogenation to methanol. *Mol. Catal.* **2021**, *509*, 111641. [[CrossRef](#)]
26. Jiang, L.; Zhu, H.W.; Razzaq, R.; Zhu, M.L.; Li, C.S.; Li, Z.X. Effect of zirconium addition on the structure and properties of CuO/CeO₂ catalysts for high-temperature water-gas shift in an IGCC system. *Int. J. Hydrog. Energy* **2012**, *37*, 15914–15924. [[CrossRef](#)]
27. Liu, Y.J.; Li, Z.F.; Xu, H.B.; Han, Y.Y. Reverse water-gas shift reaction over ceria nanocube synthesized by hydrothermal method. *Catal. Commun.* **2016**, *76*, 1–6. [[CrossRef](#)]
28. Gao, D.; Yang, G.; Li, J.; Zhang, J.; Xue, D. Room-Temperature Ferromagnetism of Flowerlike CuO Nanostructures. *J. Phys. Chem. C* **2010**, *114*, 18347–18351. [[CrossRef](#)]
29. Hoch, L.B.; Wood, T.E.; O'Brien, P.G.; Liao, K.; Reyes, C.A.M.; Ozin, G.A. Photomethanation of Gaseous CO₂ over Ru/Silicon Nanowire Catalysts with Visible and Near-Infrared Photons. *Adv. Sci.* **2014**, *1*, 1400001.
30. Xiong, K.; Zhou, G.L.; Zhang, H.D.; Shen, Y.; Zhang, X.M.; Zhang, Y.H.; Li, J.L. Bridging Mo₂C-C and highly dispersed copper by incorporating N-functional groups to greatly enhance catalytic activity and durability for the carbon dioxide hydrogenation. *J. Mater. Chem. A* **2018**, *6*, 15510–15516. [[CrossRef](#)]
31. Wang, L.C.; TahvildarKhazaneh, M.; Widmann, D.; Behm, R.J. TAP reactor studies of the oxidizing capability of CO₂ on a Au/CeO₂ catalyst-A first step toward identifying a redox mechanism in the Reverse Water-Gas Shift reaction. *J. Catal.* **2013**, *302*, 20–30. [[CrossRef](#)]
32. Midya, A.; Ghorai, A.; Mukherjee, S.; Maiti, R.; Ray, S.K. Hydrothermal growth of few layer 2H-MoS₂ for heterojunction photodetector and visible light induced photocatalytic applications. *J. Mater. Chem. A* **2016**, *4*, 4534–4543. [[CrossRef](#)]
33. Pan, X.N.; Xi, B.J.; Lu, H.B.; Zhang, Z.C.; An, X.G.; Liu, J.; Feng, J.K. Molybdenum Oxynitride Atomic Nanoclusters Bonded in Nanosheets of N-Doped Carbon Hierarchical Microspheres for Efficient Sodium Storage. *Nano-Micro Lett.* **2022**, *10*, 154–169.
34. Zhang, S.; Zeng, Y.W.; Wang, Z.T.; Zhao, J.; Dong, G.D. Glycerol-controlled synthesis of MoS₂ hierarchical architectures with well-tailored subunits and enhanced electrochemical performance for lithium ion batteries. *Chem. Eng. J* **2018**, *334*, 487–496. [[CrossRef](#)]
35. Gao, P.; Li, F.; Zhan, H.; Zhao, N.; Xiao, F.; Wei, W.; Zhong, L.; Wang, H.; Sun, Y. Influence of Zr on the performance of Cu/Zn/Al/Zr catalysts via hydrotalcite-like precursors for CO₂ hydrogenation to methanol. *J. Catal.* **2013**, *298*, 51–60. [[CrossRef](#)]
36. Wang, L.; Fang, W.; Xiao, F.S. NbOPO₄ supported Rh nanoparticles with strong metal-support interactions for selective CO₂ hydrogenation. *ChemSusChem* **2020**, *13*, 6300–6306.
37. Zhou, Z.; Kong, Y.; Tan, H.; Huang, Q.W.; Wang, C.; Pei, Z.X.; Wang, H.Z.; Liu, Y.Y.; Wang, Y.H.; Li, S.; et al. Cation-Vacancy-Enriched Nickel Phosphide for Efficient Electrosynthesis of Hydrogen Peroxides. *Adv. Mater.* **2022**, *34*, 2106541. [[CrossRef](#)]
38. Bobadilla, L.F.; Santos, J.L.; Ivanova, S.; Odriozola, J.A.; Urakawa, A. Unravelling the Role of Oxygen Vacancies in the Mechanism of the Reverse Water-Gas Shift Reaction by Operando DRIFTS and Ultraviolet-Visible Spectroscopy. *ACS Catal.* **2018**, *8*, 7455–7467. [[CrossRef](#)]
39. Liu, Y.X.; Li, L.W.; Zhang, R.Y.; Guo, Y.H.; Wang, H.; Qingfeng Ge, Q.F.; Zhu, X.L. Synergetic enhancement of activity and selectivity for reverse water gas shift reaction on Pt-Re/SiO₂ catalysts. *J. CO₂ Util.* **2022**, *63*, 02128. [[CrossRef](#)]
40. Da, B.; Zhou, G.; Ge, S.; Xie, H.; Jiao, Z.; Zhang, G. CO₂ reverse water-gas shift reaction on mesoporous M-CeO₂ catalysts. *Can. J. Chem. Eng.* **2017**, *95*, 634–642. [[CrossRef](#)]
41. Tarifa, P.; Gonzalez-Castano, M.; Cazana, F.; Arellano-García, A.M.H. Development of one-pot Cu/cellulose derived carbon catalysts for RWGS reaction. *Fuel* **2022**, *319*, 123707. [[CrossRef](#)]
42. Yang, L.; Pastor-Pérez, L.; Villora-Pico, J.J.; Gu, S.; Sepúlveda-Escribano, A.; Reina, T.R. CO₂ valorisation via reverse water-gas shift reaction using promoted Fe/CeO₂-Al₂O₃ catalysts: Showcasing the potential of advanced catalysts to explore new processes design. *Appl. Catal. A-Gen.* **2020**, *593*, 117442. [[CrossRef](#)]

Disclaimer/Publisher's Note: The statements, opinions and data contained in all publications are solely those of the individual author(s) and contributor(s) and not of MDPI and/or the editor(s). MDPI and/or the editor(s) disclaim responsibility for any injury to people or property resulting from any ideas, methods, instructions or products referred to in the content.